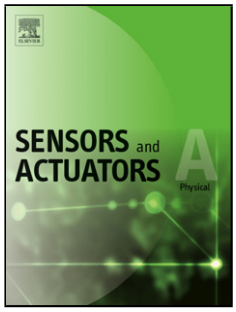

Design and optimization of an opto-acoustic sensor based on porous silicon phoxonic crystals

L. Forzani, C.G. Mendez, R. Urteaga, A.E. Huespe

PII: S0924-4247(21)00380-0

DOI: https://doi.org/10.1016/j.sna.2021.112915

Reference: SNA 112915

To appear in: *Sensors and Actuators: A. Physical*

Received Date: 11 January 2021

Revised Date: 19 May 2021

Accepted Date: 10 June 2021

Please cite this article as: { doi: https://doi.org/

Design and optimization of an opto-acoustic sensor based on porous silicon phoxonic crystals

L. Forzani[1,2]*, C. G. Mendez[1], R. Urteaga[2,3], A. E. Huespe[1,3]

[1]CIMEC-UNL-CONICET, Predio Conicet Dr Alberto Cassano, CP 3000 Santa Fe, Argentina

[2]IFIS, UNL-CONICET, Güemes 3450, Santa Fe, CP, 3000, Argentina

[3]FIQ-UNL, Santiago del Estero 2800, Santa Fe, CP, 3000, Argentina

May 19, 2021

Abstract

We present the theoretical study of an opto-acoustic microdevice, a phoxonic crystal, made of porous silicon with a specific acoustic response in the range of tens of MHz and optical response in the visible and near-infrared range. We propose to control the opto-acoustic response of this device by spatially modulating the microstructure porosity. Based on this study, a multilayer microcavity is designed to have a strong coupling between the acoustic and optical response. The coupling mechanism is generated by exploiting the structural resonance due to the acoustic waves which produce maximum mechanical strains at the center of the cavity. The associated mechanical deformations of the central cavity change the optical response of the multilayer, allowing the mechanical response to be detected using optical techniques. In a phoxonic crystal, the acoustic and optic central gap frequencies are determined by the multilayer configuration which imposes a fixed relation between both resonant frequencies. This feature establishes a challenge for the microdevice design. To mitigate this problem, two microcavities, one inside the other in a Matryoshka-like configuration is here

*Corresponding author. E-mail address: luisina.forzani@santafe-conicet.gov.ar (L. Forzani).

proposed, placing an optical microcavity into the spacer of an acoustic microcavity. Consequently, the localized acoustic field generates a high perturbation of the optical microcavity structure. The optical microcavity is tuned at near-infrared frequencies, while the larger acoustic microcavity resonates at acoustic frequencies of the order of tens of MHz. The microdevice is designed to display a high optical response induced by acoustic deformation. Optical sensitivity to this effect is used to design a multiparametric sensor. Thanks to the porous structure of the device, it is possible to build a transducer sensitive to the presence of analytes in the environment that affect both its mechanical and optical response.

Keywords: Porous Silicon, opto-acoustic device, opto-acoustic metamaterial, phoxonic crystal.

1 Introduction

Porous silicon (PS) is a very versatile material to construct photonic crystals formed by a sequence of PS layers of adjustable thicknesses and porosities in a wide range of values, with a highly tunable optical responses [1]. This characteristic permits the construction of microdevices such as rugate filters [2], distributed Bragg reflectors (DBR) [3], or optical microcavities [4] displaying sharp resonances in the stopping bands. In a DBR, multiple alternating layers of different porosities give a high reflectivity for certain optical wavelengths due to the net effect of the multiple reflections at the interfaces between layers. By increasing the porosity contrast or using a greater number of periods of alternating layers, a greater reflectance will be obtained at the central wavelength. In particular, in this work, we are interested to study PS multilayer microcavities, conformed by two DBR, separated by one layer with a larger thickness (defect or central cavity).

The central resonance frequency in a photonic crystal depends on the optical characteristics of the microstructure [1]. Besides, the porous structure of PS allows direct contact of the internal microstructure with the environmental variables. Both features can be utilized to build highly sensitive sensor devices based on measuring the changes of the environmental dielectric constants in the porous of the microstucture [5].

Following a similar strategy, phononic crystals have been designed with a specific acoustic response displaying a sharp resonance peak at some given target characteristic frequency [6, 7]. The central resonance frequency of a phononic

crystal depends on the mechanical characteristics of the microstructure. Therefore, PS sensors can also be built that measure changes in acoustic impedances when interacting with the environment. However, phononic crystals exploiting the sharp peak at the resonance frequency jointly with the porous character of the microstructure have not been widely employed yet. Probably, this situation is due to the difficulties to measure the acoustic response at high frequencies, which requires complex equipment [8]; or due to the necessity of placing detectors in direct contact with the multilayers that hinders the interaction with the environment [7]. In this direction we mention the works of [9, 10, 11], where the authors propose an opto-acoustic microcavity alternating layers of different materials. As the layers are not porous, it disables the use of this device as a sensor due to the interior of the device is not in contact with the environment. On the other hand, in these works the use as a sensor is not exploited and the construction part is different.

In this work, we design a multiparametric PS sensor that couples the optical and acoustic responses. Consequently, changes of both responses due to variations of environmental variables, either dielectric constants or mechanical impedances, can be sensed by only assessing the optical response. This feature can be attained by manufacturing a microdevice constituted by a phononic and photonic crystal (phoxonic crystal) [12] based on a PS microcavity (figure 1). Phoxonic crystals are dual phononic/photonic crystals simultaneously exhibiting band gaps for both types of excitations. Additionally, phonons and photons can be confined in the same cavity, which enhances their interactions. The confining ability of the microcavity is quantified through the quality factor Q, defined as $Q = \lambda_0/\Delta\lambda$, where λ_0 is the central resonance frequency and $\Delta\lambda$ is the full width at half maximum (FWHM) of the mode amplitude (figure 2) [13].

However, the design of a PS phoxonic crystal following this concept suffers from several issues:

i The thicknesses of the PS layers in a DBR device have to be of the order of $\lambda_0/4$. Thus, in the range of the infrared light, where Si is transparent, the thicknesses of the layers are of the order of 200-400 nm. These layer thicknesses imply that the acoustic DBR would resonate at frequencies of the order of 3-8 GHz. However, the acoustic attenuation in PS increases strongly with frequency, which induces an appreciable loss of transmittance in this frequency range.

ii The acoustic microcavity factor Q could be augmented by increasing the number of DBR periodic layers. But, the increment of the number of peri-

odic layers is limited by the total thickness of the silicon wafer. A decrease in the resonant frequency reduces acoustic attenuation but also decreases the number of periods in the DBR.

iii The factor Q can be increased by increasing the porosity contrast between layers; however, the acoustic attenuation also increase with the Si porosity [7], inducing again a decrease of Q.

These issues establish a challenge to build PS multilayers with similar acoustic and optical thicknesses having sharp acoustic central resonance frequencies and strong opto-acoustic coupling effect.

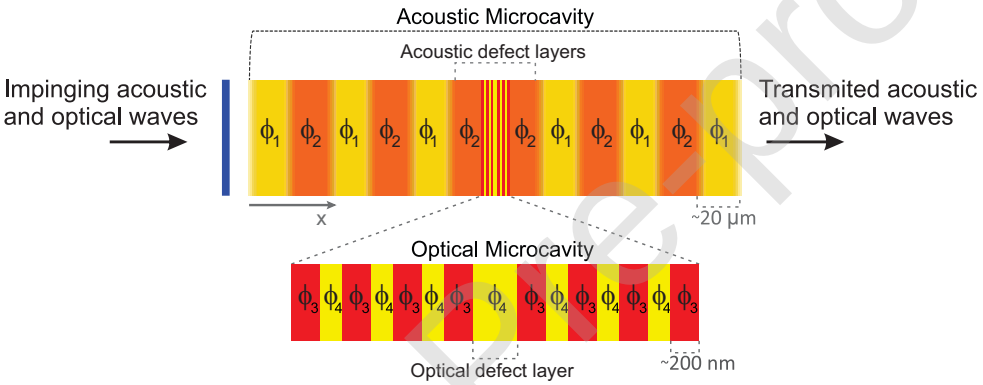

Figure 1: One-dimensional phoxonic crystal scheme. An optical microcavity (a PS multilayer with porosities ϕ_3 and ϕ_4) is placed inside an acoustic microcavity (a PS multilayer with porosities ϕ_1 and ϕ_2) in a Matryoshka-like configuration.

We propose an alternative design consisting of two PS multilayer microcavities coupled in a Matryoshka-like configuration, such as sketched in figure 1. We incorporated an optical microcavity that resonates in the near infrared range placed within a larger acoustic microcavity that resonates at acoustic frequencies much lower than 1 GHz. The minimum acoustic frequency that can be attained in this case is limited by the Si wafer thickness taken to build the PS multilayer microdevice. Consequently, we search for the optimum number of periodic layers and the porosity contrast between layers to obtain the maximum possible optic-acoustic coupling. A further experimental advantage of adopting this configuration is that the generation of acoustic waves in the MHz range can be carried out without the need of complex equipment. In this sense, the excitation acoustic wave can be generated by constructing a piezoelectric layer on the multilayer

structure [14], or coupling a thermophone that can be built directly on the porous layer [15, 16, 17].

This matryoshka type configuration was reported by [18], but unlike our proposal, the authors designed an optical microcavity that contains an acoustic microcavity within its defect.

2 Theory

We study the case of an acoustic wave impinging normally the layers of the PS microdevice, and therefore, longitudinal acoustic waves travelling across the PS layers are considered. Beside, we assume that the porous sizes are smaller than the optical and acoustic wavelength, which allows to adopt optical and acoustic properties resulting from an effective medium theory.

The porosities, ϕ, and the thicknesses, d, of the PS layers are created during the anodizing process of a silicon wafer through an appropriate current profile. With this technique, it is possible to produce PS one-dimensional (1D) photonic/phononic crystals by generating multilayers with alternated optical refractive indices $n(\phi)$ or acoustic impedances $Z(\phi)$, respectively.

The acoustic impedance in a medium is defined as $Z = \rho v$, where ρ and v are the density and the velocity of sound in this medium. In particular, for porous silicon, ρ and v depend on the porosity ϕ as follows: $\rho(\phi) = \rho_{Si}(1-\phi)$ and $v(\phi) = v_{Si}(1-\phi)^{\kappa}(1+0.16\phi)^{-1/2}$, where the density of silicon, ρ_{Si}, is $\rho_{Si} = 2329 kg/m^3$, and the sound of the longitudinal velocity in silicon for [100] direction, v_{Si}, is $v_{Si} = 8433 m/s$. The exponent κ depends on the porous silicon morphology and is between 0.5 and 1 [6, 7].

A periodic system of alternating layers (DBR) gives a high reflectivity for certain wavelengths due to the net effect of multiple partial reflections at the interfaces between layers. If the thickness of each layer of the phononic DBR is

$$d_a(\phi) = \frac{Z(\phi)}{4 f_a \rho(\phi)}\,, \tag{1}$$

the microstructure has a resonant frequency $f_a = c_s/\lambda_a$, where c_s is the sound velocity in air and λ_a is the central wavelength of the DBR.

If a central defect of thickness $2d_a$ is introduced in the DBR, a microcavity with a sharp resonance at λ_a is obtained [1]. In complete analogy with phononic DBR, it is possible to obtain a photonic DBR resonating at frequency f_o if the

thicknesses of the layers are taken as

$$d_o(\phi) = \frac{c}{4 f_o n(\phi)}\,, \tag{2}$$

where c is the speed of light. The optical resonant wavelength can be calculated as $\lambda_o = c/f_o$ and the refractive index $n(\phi)$ of the PS layers can be estimated using an effective medium mixing model. In this work we use the effective medium approximation of Landau-Lifshitz/Looyenga. The refractive indices of PS are in the range of 1.4-2.1 for porosities between 80% and 50% respectively [19].

Optical microcavities made of PS with resonance modes (λ_o) in infrared have shown excellent performances due to the low extinction coefficient of porous silicon mainly limited by scattering processes [20, 21]. For the calculation of the refractive indices, we took into account the fundamental absorption of bulk silicon [22]. And also, in the IR range, we incorporated the optical absorption due to the scattering effects (of $146 cm^{-1}$) obtained experimentally by [21].

To calculate the optical transmittance at normal incidence of the PS multilayers, we use the matrix transfer method [23]. Beside, when only pure longitudinal waves exist, the same transfer matrix method can be used to calculate the acoustic transmittance by replacing $n(\phi)$ with the acoustic admittance $1/Z(\phi)$ [24, 25, 6].

2.1 Mechanical strains

The mechanical strains produced by the acoustic wave modify the geometry of the optical cavity generating, in turn, a change of the device optical response. In this way, the acoustic pressure in the microcavity modulates the optical response of the device.

The mechanical strains, generated by the incident acoustic wave, are amplified in the center of the cavity due to the multiple reflections between the layers. The total displacements in each layer can be calculated as $u_{tot}(x) = -i[v(x) + v'(x)]/\omega$ with ω, $v(x)$ and $v'(x)$ being the wave angular frequency, the velocities of the incident and reflected waves respectively [24, 25]. The strain are the symmetric gradient of u_{tot}, resulting $\varepsilon = (\partial u_{tot}(x))/\partial x = -\rho_j/Z_j[v(x) - v'(x)]$.

Then, the mechanical strains can be evaluated using the transfer matrix method through the displacements. According to this methodology, the transfer matrix of the $i-$th layer can be calculated as follows

$$\bar{\bar{T}}_i = \begin{bmatrix} \cos(k_i d_i) & iZ_i \sin(k_i d_i) \\ i\frac{\sin(k_i d_i)}{Z_i} & \cos(k_i d_i) \end{bmatrix}\,, \tag{3}$$

were k_i, Z_i and d_i are the complex wave number, the characteristic impedance and the thickness of the i-th layer, respectively [24].

Thus, the normalized strain ε_j at the $j-$th layer is computed with the following expression:

$$\frac{\varepsilon_j}{p_0} = -\frac{\rho_j}{Z_j^2}\left([T^{-1}]_{11}(1+r) + [T^{-1}]_{12}\frac{1-r}{Z_0}\right), \tag{4}$$

where p_0 is the incident wave pressure, Z_0 is the air impedance, r is the reflectance coefficient. The transfer matrix $[T]$ is computed as the product of the transfer matrices of the successive PS layers: $T = \prod_{i=1}^{i=j-1} \bar{\bar{T}}_i$. The components $(1,1)$ and $(1,2)$ of the inverse of the transfer matrix are denoted by $[T^{-1}]_{11}$ and $[T^{-1}]_{12}$, respectively.

The main objective of this work is to optimize the opto-acoustic coupling by searching for the maximum value of the normalized mechanical strain at the cavity center for different structural configurations.

2.2 Acoustic attenuation

Besides of the optical losses, a determinant factor of the opto-acoustic coupling in the microcavity is the acoustic attenuation. Therefore, this effect must be assessed in detail for the designed phoxonic device. The acoustic losses are taken into account by including the imaginary term of the wave number k in the transfer matrix T. Then, the wave number in the j-th layer is defined as: $k_j = \omega/v_j + i\alpha_j$, being α_j the acoustic attenuation coefficient of the respective layer.

The dominant acoustic attenuation mechanism in semiconductors and insulators is Akhiezer damping, but there are also other mechanisms such as thermoelastic [26, 27, 28]. The longitudinal attenuation coeficient of the silicon bulk for [100] direction is $\alpha_{Si} \approx 9.32 dB/(cmGHz^2)$ at 300 K and $f_a = 1GHz$ [29, 28, 7].

Additionally, we consider the attenuation coefficient of porous silicon as:

$$\alpha(\phi)[\frac{Np}{m}] = \alpha_{Si}(1-\phi)^{(\beta-\kappa)}(1+0.16\phi)^{\frac{5}{2}}\frac{(1+(\omega\tau_{Si})^2)}{(1+(\omega\tau)^2)}, \tag{5}$$

where $\kappa = 0.53$ and β are parameters associated to the PS morphology [30, 7]. The parameter β can vary between 1.3 and 2.05, depending on the doping of the silicon wafer. It is closer to 1.3 for Si type p and closer to 2.05 for Si type n. the relaxation time of the porous silicon layer, τ, is $\tau \approx \tau_{Si}(1-\phi)^{\beta}(v_{Si}/v)^2$ [7].

Given that $\omega\tau \ll 1$ in the working range of frequencies, the attenuation α_{Si}, and therefore α, shows a quadratic dependence on frequency. This response strongly penalizes the maximum acoustic strains that could be attained at the central resonance frequency in the device. Furthermore, the attenuation coefficient is affected by the porosity and the morphological parameter β. When the porosity increases, as well as, when the parameter β decreases, the coefficient α increases. In the calculations, we use $\beta = 1.7$ and a sensitivity analysis of this parameter is performed in section 3.

2.3 Microcavity design

We propose to incorporate an optical microcavity inside of an acoustic cavity to generate a strong coupling between the mechanical and optical responses.

As it is explained in section 1, a trade-off arises between the number of periods in the DBR and the attenuation due to the limitation of a maximum thickness of the silicon wafer used to construct the device. At high frequencies, it is possible to design a multilayer structure with a larger number of periods (and therefore thinner layers) that increases the number of constructive reflections in the microcavity. However, the acoustic attenuation has a greater negative effect on the capacity of the microcavity to maximize the acoustic strain in the cavity. Therefore, we search the optimal central acoustic frequency, f_a, minimizing the attenuation effect while keeping, as high as possible, the number of periods of the DBR.

Additionally, certain experimental limitations have to be consider when designing the PS multilayer. For example, the range of porosities that can be obtained in a laboratory depends on the silicon doping and is typically between $50\% \leq \phi \leq 80\%$ [1].

Let us consider, for example, a 12-period DBR constructed on a typical silicon wafer of thickness $625\mu m$. Then, the maximum possible value for the individual layers is about $d_a = 25\mu m$ (equation (1)), which imposes a minimum value for $f_a \approx 60MHz$. If the microcavity itself is intended to be acoustically resonant, ($d_o = d_a$), the optical resonance occurs at $\lambda_o = 210\mu m$. Otherwise, if the layer thicknesses are chosen to obtain λ_o in the near-infrared spectrum, where the silicon is transparent, the d_o values results of about $200nm$ (for $\lambda_o \approx 1.5\mu m$) and f_a will be in the order of $8GHz$. Therefore, it is not possible to construct a simple microcavity that optically is in the range of near-infrared and, at the same time, acoustically is in the range of tens of MHz for the first order gap. The idea to use a Matryoshka-like configuration, as shown in figure 1, solves this problem since it allows to build an acoustic microcavity working at low frequencies with

an internal optical microcavity working in the near-infrared range.

Furthermore, the Matryoshka-like architecture enables the acoustic response to be determined by optical measurements. The coupling between both responses occurs because a mechanical deformation of the optical microcavity modifies the optical thickness of the structure and therefore shifts the optical resonance wavelength. The optical transmission spectrum varies periodically in time with the period of the acoustic wave.

Figure 2 schematizes a snapshot of the optical transmittance shift due to acoustic strains of the optical microcavity.

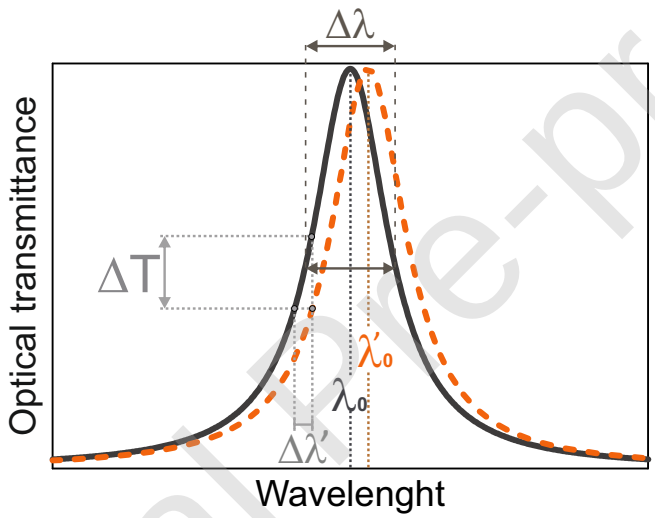

Figure 2: The optical transmittance shift due to the acoustical wave in the optical microcavity central layer.

The optical transmittance resonance is very sensitive to the contrast of layer porosities and the number of periods that forms the lateral DBR's. The quality factor ($Q_o = \lambda_o/\Delta\lambda$) of the opto-acoustic microcavity is determined by contrast of the the refractive index profile and by the number of layers.

Furthermore, a deformation of the structure due to the acoustic wave produces a peak shift amplitude $\Delta\lambda^{'} = \lambda_o^{'} - \lambda_o$. Due to this shift, the optical transmittance on one side of the peak shows a change of amplitude ΔT, such as depicted in figure 2, which can be used to measure the acoustic deformation of the microcavity. In consequence, the coupling in the microcavity may be determined by the relative change of the optical transmittance produced by the acoustic input pressure

$\Delta T/p_0$. From definition of the optical quality factor Q_o, and considering small variations of the peak position, we have that $\Delta T \propto \frac{\Delta\lambda'}{\Delta\lambda} = \Delta\lambda' \frac{Q_o}{\lambda_o}$. Since the strain in the microcavity is equal to the relative shift of the microcavity resonance, i.e. $\varepsilon = \frac{\Delta\lambda'}{\lambda_o}$[9], then $\Delta T \propto Q_o \varepsilon$.

Considering this relationships, we introduce a parameter that measures the coupling between optical an acoustical responses. This coupling factor parameter is defined as follows

$$S = \frac{Q_o \varepsilon}{p_0} \,. \tag{6}$$

Note that for the central cavity layer, the ratio $\frac{\varepsilon}{p_0}$ can be calculated using equation (4).

Considering a transmittance peak with a Lorentzian profile and unit amplitude, the maximum change in transmittance produced by the acoustic wave of amplitude p_0 can be calculated as

$$\Delta T = S p_0 \,. \tag{7}$$

2.3.1 The opto-acoustic device as an environmental sensor

Given the porous structure of the device, a change in the environment due to the presence of a analyte that enters the device produces a refractive index variation of the multilayer. This change produce a constant shift of the transmittance peak that can be used as a transductor to measure the analyte concentration [5]. Alternatively, the presence of an analyte can also modify the effective acoustic impedance of the multilayer, causing the resonant frequency of the device to change [11]. Given the acoustic-optical coupling of the device, the resonance frequency can be monitored by measuring the optical transmittance oscillation at the acoustic wave frequency (Eq. 7). In this way the device can also be used as a transducer sensitive to the acoustic properties of the analyte. Finally, both determinations (acoustic and optical) can be performed simultaneously in this device, so the proposed scheme could be used to obtain complementary information for the determination of a single analyte. Another possibility that opens up for this multiple sensor is to discriminate a mixture of different analytes from the modification they produce in the optical and acoustic response of the sensor.

2.3.2 Smooth porosity transition between acoustic layers

Taking advantage of the fact that the optical and acoustic microcavities have significant different sizes, it is possible to minimize the interference produced by the optical reflections on the interfaces of the acoustic microcavity by introducing a smooth porosity transition between layers of the acoustic microcavity. This arrangement is adopted to avoid interference in the optical performances caused by the optical reflections produced by the abrupt changes of the refraction indices in the layer interfaces. We use a transition layer similar to an Epstein profile [31] of width δ, schematized in figure 3.

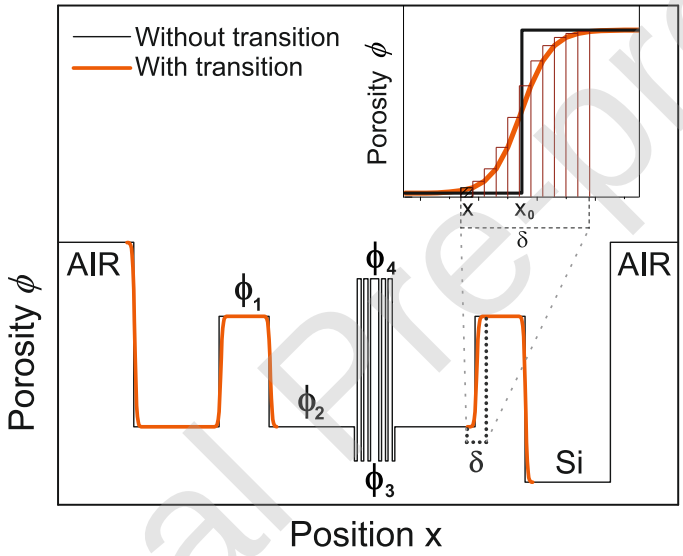

Figure 3: Schematic spatial distribution of porosities in the acoustic microcavity with and without smoothing. In the insert: porosity smoothing detail of two successive acoustic layers with the Epstein-like profile.

The transition zone is subdivided in 40 uniform sub-layers with a spatial distribution of porosities given by:

$$\phi(x) = \sqrt{\frac{1}{2}\left(\phi_1^2 + \phi_2^2 + (\phi_2^2 - \phi_1^2)\tanh\left[\frac{2(x-x_0)}{\delta}\right]\right)}, \tag{8}$$

where ϕ_1 and ϕ_2 are the porosities at both sides of the interface located at position x_0. With this porosity distribution, and assuming that $\delta \gg \lambda_o$ is satisfied, a negligible optical reflection is produced in the acoustic layer interfaces. Furthermore,

the condition $\lambda_a \gg \delta$ must be verified to allow acoustic reflection in the layers that form the acoustic microcavity. In the first layer, an Epstein-like profile with porosity from 100% to the porosity of the first acoustic layer is added to smooth the difference between the air impedance and the first PS layer impedance.

Considering the acoustic wave propagation direction, the last layer of the device, on the side where the wave exits from the phoxonic crystal, is formed by the remaining crystalline silicon of the wafer (Si_c). The thickness of this layer is also chosen to be equivalent to 1/4 of the resonance wavelength of the acoustic microcavity.

2.3.3 Optimal multilayer configuration

The factor S is taken as the objective function to optimize the microcavity design. Thus, we look for the best combination of parameters providing an optimal value of S, with the highest possible Q_o factor and the maximum acoustic deformation at the center of the optical defect. According to this design criterion, the system would have the maximum sensitivity to detect small changes produced by acoustic vibrations.

The space of parameters of this optimization problem, which characterize the optical and acoustic microcavities, are ϕ_1, ϕ_2, ϕ_3, ϕ_4, δ and the number of periods of the DBRs in both microcavities.

Based on the previous analysis, we discuss two particular multilayer configurations:

Configuration A:

$$\underbrace{(\phi_1\ \phi_2)_n}_{\text{left acoustic DBR}}\ \underbrace{(\phi_3\ \phi_4)_m\ (\phi_4\ \phi_3)_m}_{\text{Optical microcavity}}\ \underbrace{(\phi_2\ \phi_1)_n}_{\text{right acoustic DBR}}\ \underbrace{Si_c}_{\text{substrate}}$$

Configuration B:

$$\underbrace{\phi_2\ (\phi_1\ \phi_2)_n}_{\text{left acoustic DBR}}\ \underbrace{(\phi_3\ \phi_4)_m(\phi_4\ \phi_3)_m}_{\text{Optical microcavity}}\ \underbrace{(\phi_2\ \phi_1)_n}_{\text{right acoustic DBR}}\ \underbrace{Si_c}_{\text{substrate}}$$

The terms in parentheses represent a periodic sequence of two layers with the indicated porosities. The subscripts n and m indicate the number of sequence repetitions in the acoustic and optical microcavities respectively. The structures of both configurations are supported by the silicon substrate.

Note the symmetric arrangement of both DBRs in Configuration A, while the left DBR in Configuration B has one additional layer with porosity ϕ_2 respect

to the right DBR. The right layer of Si_c has the thickness: $v_{Si}/(4f_a)$ and plays the role of increasing the acoustic resonance inside the cavity. Also, note that in both configurations, the central layer of the optical microcavity is constructed with porosity ϕ_4, while the central layer of the acoustic microcavity, containing the optical microcavity, is constructed with porosity ϕ_2.

Additionally, because the minimum attenuation is achieved at lower frequencies, both Configurations A and B are constrained to occupy the full Si wafer thickness d_{Si}. Therefore, the frequency f_a results from imposing the parameters n, ϕ_1, ϕ_2 and the thickness of the Si wafer.

3 Results and discussions

As mentioned in the previous section, the design objective is to optimize the function S, defined in equation (6), which implies maximizing the product $Q_o\varepsilon$. The optical response of the system (Q_o) is mainly determined by the parameters of the central microcavity (ϕ_3, ϕ_4 and m). The use of a transition region at the interfaces between the layers that form the acoustic microcavity (porosities ϕ_1 and ϕ_2), eliminates the influence of this interface on the optical response. The adopted value $\delta = 4\mu m$ satisfies the conditions: $\lambda_a \gg \delta \gg \lambda_o$ for several tested configurations of the acoustic central gap frequency: from f_a $5MHz$ ($\lambda_a = 68\mu m$) to $60MHz$ ($\lambda_a = 6\mu m$) , and optically are used $\lambda_o = 1.5\mu m$. We corroborate that the factor Q_o becomes independent of the acoustic microcavity configuration without producing noticeable changes in the acoustic response of the system. Furthermore, Q_o increases with the number of periods m, however, the roughness of the layers limits the maximum value that can be experimentally obtained [32]. The highest values of Q_o that have been obtained using porous silicon are 2000-3400 [20, 21], which can be reached using a value of $m \sim 18-20$ respectively. Taking into account these limitations, we choose as design parameter $m = 18$, and ϕ_3 and ϕ_4 with the higher contrast (50% and 80% respectively). The maximum strain in the defect layer is reached when the softer layer is placed in this position and is built with the maximum admissible porosity $\phi_4 = 80\%$ (the manufacturing upper limit of the porosity). Further, the maximum Q-factor is attained with the maximum porosity contrast between two successive optical layers. This means that the lower admissible porosity $\phi_3 = 50\%$ is the optimum one for the stiffer layer. Finally, we use a resonance wavelength in the infrared, where porous silicon is transparent. Throughout this work, we use $\lambda_o = 1.5\mu m$.

Also, the strain ε is expected to increase with the number of periods n and with

the porosity contrast increment (ϕ_1 and ϕ_2). However, this effect is not evident because, as previously mentioned in sub-Section 2.3, an increment of n implies a thinner layers, and therefore an increment of the acoustic frequency as well as an increment of the acoustic attenuation at the resonant frequencies. To assess the contradictory effect on S due to a change of the parameter n, we test the configurations A and B using the admitted extreme values of porosity, 50% and 80%. These extreme values are assigned to ϕ_1 and ϕ_2 in all the possible combinations.

Figure 4 shows the results attained with this assessment. It shows the function S in terms of the number of periods n. As n increases and simultaneously the thickness of the layers decreases, the acoustic transmittance peak shifts at higher resonance frequencies. That is, each analyzed configuration has a different f_a. Note that configurations with the lower porosity in the acoustic central cavity ($\phi_2 = 50\%$) gives the higher coupling factor. Furthermore, configuration B with $\phi_2 = 50\%$ and $n = 1$ has the highest coupling factor. Anyway, configuration A with $n = 2$ gives a close value of S. The lowest possible frequency is obtained for $n = 0$, reaching a value of about 5MHz for configuration B. An increase in n increases the number of reflections in the microcavity and amplify the deformation, but a higher frequency also increases the attenuation, reducing the coupling efficiency. For this reason there is an optimal n value, which depends on the chosen configuration.

A similar effect on S, such as discussed in the previous paragraph, is produced by increasing the contrast of porosities between two successive layers. By increasing the contrast of porosities, Q and the acoustic attenuation increment in the acoustic cavity, as shown in equation (5). This contradictory effect of porosities contrast on S may lead to an optimal value of porosity ϕ_1, which might not be the maximum possible one. For this reason, the factor S is assessed for the best configurations obtained in figure 4, by fixing the porosity $\phi_2 = 50\%$ and testing different values of ϕ_1. The results obtained with this analysis are shown in figure 5. Figure 5 shows the function S in terms of the porosity ϕ_1 ranging between $\phi_1 = \phi_2 = 50\%$ and the maximum admissible value $\phi_1 = 80\%$.

According to figure 4, the optimum value of S for Configuration B is found with $n = 1$. For this Configuration, the maximum S value is obtained when $\phi_1 = 73\%$, as shown in figure 5. A similar analysis for Configuration A, with $n = 2$, gives an optimum for the highest possible porosity contrast: $\phi_1 = 80\%$. Furthermore, this analysis shows that Configuration B, with $n = 1$, provides a slightly better outcome, $S = 1.2 \cdot 10^{-2}$, if compared with the optimum Configuration A.

The porosity $\phi_1 = 73\%$ in Configuration B, with $n = 1$, gives an amplification of the acoustic deformation due to the multiple reflections in the structure whereas

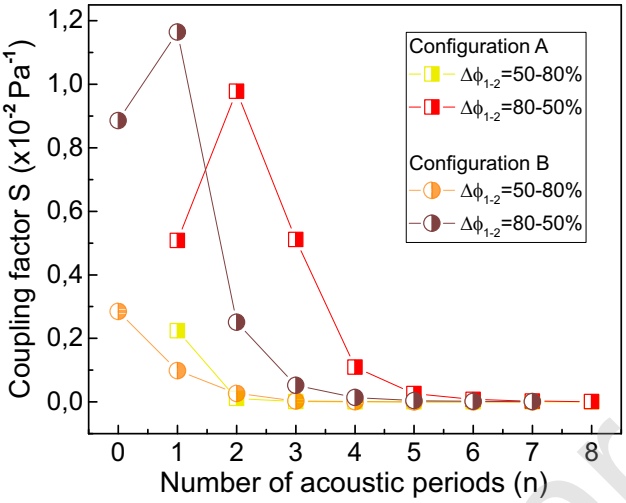

Figure 4: Coupling factor S as a function of the number of acoustic periods n for different porosity order in the layers . Each case is designed to its corresponding central resonance frequency. The notation $n = 0$ for Configuration B corresponds to a simple layer with porosity ϕ_2 on the left of the optical microcavity.

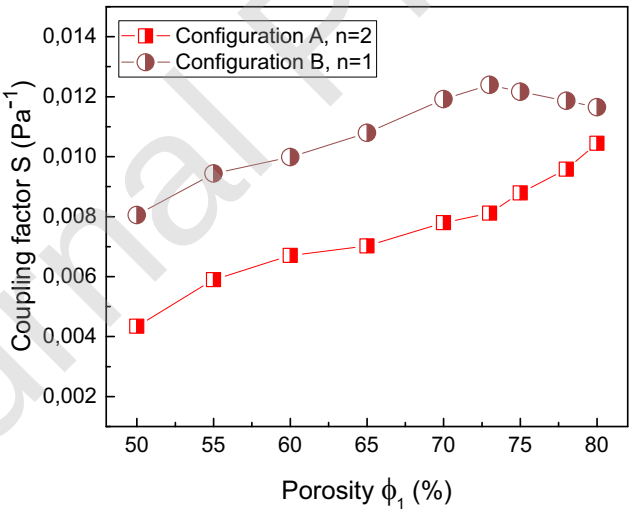

Figure 5: Optimization of the configuration A and B. The porosity ϕ_2 is fixed at 50%.

this effect does not occur for $n = 0$. In this case the acoustic central resonance frequency is about $13.2MHz$. The thicknesses of the layers are approximately $d_1 = 74\mu m$, $d_2 = 101\mu m$ and $d_{Si} = 165\mu m$. While for configuration A with $n = 2$, the acoustic microcavity is resonant at $17.7MHz$ and the thicknesses are $d_1 = 47\mu m$, $d_2 = 80\mu m$ and $d_{Si} = 117\mu m$.

Considering the obtained results, the acoustic attenuation is identified as a decisive parameter to attain an adequate coupling. The above calculations were performed by setting the morphological parameter $\beta = 1.7$ for the attenuation calculation in equation (5). To analyze the sensitivity of the result to changes in the acoustic attenuation, we calculate the variation of S in the range of reported values of β [30]. Figure 6 shows the results for three different configurations.

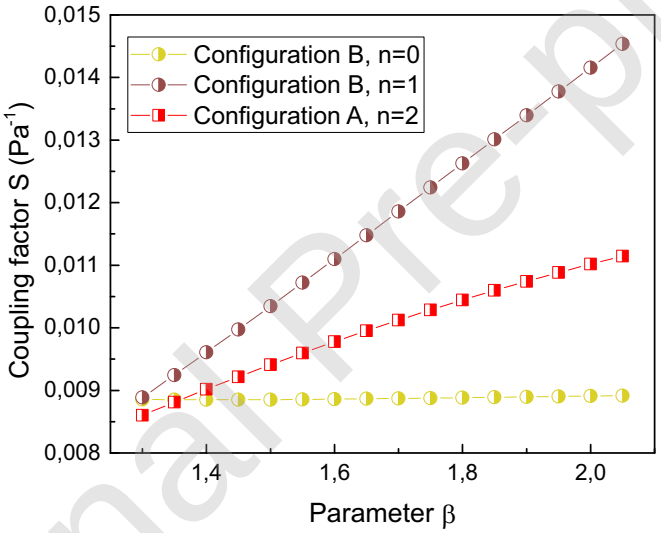

Figure 6: Sensitivity of the coupling factor S with the morphological parameter β that defines attenuation for the optimal Configurations A and B, and for the simple layer case (Configuration B with $n = 0$ and $\phi_2 = 50\%$). For configuration B with $n = 1$, we use $\phi_1 = 73\%$ and $\phi_2 = 50\%$; and for Configuration A with $n = 2$, $\phi_1 = 80\%$ and $\phi_2 = 50\%$.

We find that as β is increased, both Configurations, A with $n = 2$ and B with $n = 1$, attain higher values of S. This is because increasing the parameter β reduces the attenuation, which favors an amplification of the deformation. On the other hand, for the configuration B with $n = 0$ that works at the lowest frequency, where attenuation plays a smaller role, the value of S is almost constant. The in-

crease in the central resonance frequency obtained for higher values of n leads to an increase in the attenuation coefficient, and therefore it is more convenient to work with a reduced number of periods n.

3.1 Acoustic and optical performance of the optimal configuration

After attaining the optimal configuration (Configuration B, with $n = 1$), we analyze its uncoupled acoustic and optical response. Figure 7(a) shows the acoustic transmittance as a function of frequency and figure 7(b) shows the acoustic strains across the structure. The largest deformation in the optical cavity center occurs at the central acoustic frequency $f_a = 12.33MHz$.

Additionally, in figure 8, we show the optical transmittance (T), reflectance (R) and absorbance (A) spectrum of the double microcavity of Configuration B, with the optimum parameters and with the highest porosity contrast $\phi_3 = 50\%$, $\phi_4 = 80\%$ and using $m = 18$. A very sharp optical transmittance peak at the resonance wavelength ($\lambda_o = 1500nm$) is obtained. The quality factor of the optical microcavity is $Q_o = 2200$. The inset figure shows the transmittance peak at the resonance wavelength with (purple) and without (gray) the smooth porosity transition through the layers of the acoustic microcavity. Furthermore, by analyzing the optical transmittance peak of the isolated optical microcavity and comparing this result with transmittance peak attained with the Matryoshka-type Configuration B, we conclude that the factor Q_o is not affected by the acoustic multilayer structure.

For both studied Configurations A and B, it is possible to reach a good quality factor Q_o, of the order of 2000. However, optimized Configuration B, with a less porous layer compared with the optimized Configuration A, attains a higher factor S.

4 Conclusions

A porous silicon multilayer microdevice with a Matryoshka-type geometrical configuration is proposed in this work. It consists of two microcavities of different sizes coupling the optic and acoustic responses. The optic response is in the near-infrared range and is interacting with the acoustic response with a resonant frequency in the order of ten MHz. Following this concept and according to exper-

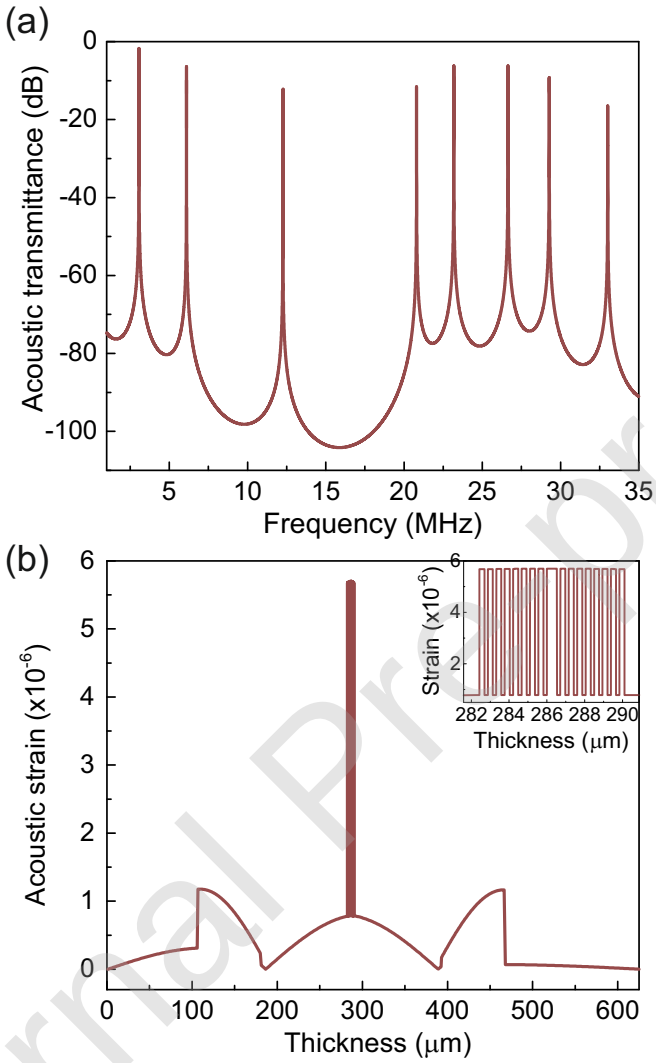

Figure 7: Acoustic response of the optimal Configuration B, with $n = 1$, $\Delta\phi_{1-2} = 73 - 50\%$, $d_1 = 74\mu m$, $d_2 = 101\mu m$, $\Delta\phi_{3-4} = 50 - 80\%$, $d_3 = 177nm$, and $d_4 = 265nm$. (a) Acoustic transmittance. (b) Acoustic deformation along the multilayer. The inset shows a detail of the optical microcavity deformation.

imental and technical limitations, a microdevice is optimally designed and simulated.

The coupling capacity of the device S depends on both variables: the opti-

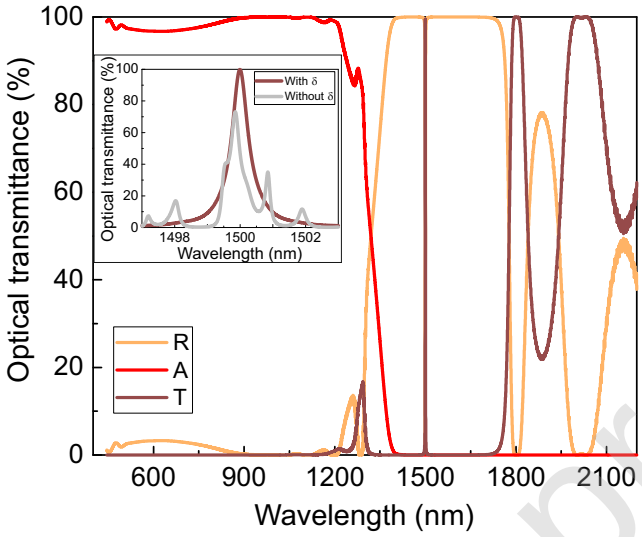

Figure 8: Optical response (reflectance (R), transmittance (T), and absorbance (A)) of the optimal opto-acoustic microcavity in terms of the wavelength (Sample with Configuration B, $n = 1$, $\Delta\phi_{1-2} = 73 - 50\%$, $d_1 = 74\mu m$, $d_2 = 101\mu m$, $\Delta\phi_{3-4} = 50 - 80\%$, $d_3 = 177nm$, and $d_4 = 265nm$). The optical quality factor of the sample is $Q_o = 2200$, and it is the same value obtained for the optical microcavity outside of the acoustic microcavity. The inset shows the transmittance peak at the resonance wavelength with (purple) and without (gray) smooth porosity transition δ.

cal quality factor Q_o and the mechanical deformation generated by the acoustic wave. The Q-factor is limited by constructive aspects, typically the roughness of the layer interfaces. Additionally, the mechanical deformation is limited by the acoustic attenuation. Since attenuation increases with acoustic frequency and the thickness of the silicon wafer imposes a constructive constraint, optimal configurations are obtained using a small number of layers in acoustic DBRs.

The assessed optimal multilayer configuration corresponds to the Configuration B, with n = 1, m = 18 and porosities $\phi_1 = 73\%$, $\phi_2 = 50\%$, $\phi_3 = 50\%$, $\phi_4 = 80\%$, and $\delta = 4\mu m$. For this optimal configuration, the value of S is approximately 0.012. This means that for acoustic pressure values that can be experimentally obtained ($p_0 \approx 1Pa$), the variation in optical transmittance is high enough to be detected with a simple optic system (a variation of $\sim 1\%$, which means an expected wavelenght shift of $\Delta\lambda' \approx 0.01nm$, see figure 2, and Eq. (6)

and (7)). Experimentally, a configuration similar to that described by Acquaroli et al. [5] could also be used to detect this small shift of the optical peak. For the operation of the device as a sensor, it is important to note the relevance of the strain magnitude at the central layer containing the optical microcavity. For this reason, the strain magnitude at that site is important to define the performance of the sensor. Additionally, it is interesting to note that the strain phase could be studied as an extra element providing more information about the analyte to be sensed.

Finally, the sensitivity of the PS to different analytes, due to variations in the ultrasonic signal transduction, is an important characteristic of this microdevice that has to be highlighted. This characteristic can be exploited to build an efficient optic-acoustic deformation transducer, sensitive to changes in the environment. Thus, it opens new possibilities to attain sensors combining optical and acoustic responses and allowing for the design of new opto-acoustic sensors.

References

[1] L. Canham. Handbook of porous silicon. Springer, 2014.

[2] M.J. Sweetman and N.H. Voelcker. Chemically patterned porous silicon photonic crystals towards internally referenced organic vapour sensors. RSC advances, 2(11):4620–4622, 2012.

[3] G. Barillaro. Porous silicon optical biosensors. In Leigh Canham, editor, Handbook of porous silicon. Springer, 2014.

[4] G. Shtemberg and E. Segal. Porous silicon optical biosensors. In Leigh Canham, editor, Handbook of porous silicon. Springer, 2014.

[5] L.N. Acquaroli, R. Urteaga, and R.R. Koropecki. Innovative design for optical porous silicon gas sensor. Sensors and Actuators B: Chemical, 149(1):189–193, 2010.

[6] G.N. Aliev, B. Goller, D. Kovalev, and P.A. Snow. Hypersonic acoustic mirrors and microcavities in porous silicon. Applied Physics Letters, 96(12):124101, 2010.

[7] G.N. Aliev and B. Goller. Hypersonic phononic stopbands at small angles of wave incidence in porous silicon multilayers. Journal of Physics D: Applied Physics, 48(32):325501, 2015.

[8] L.C. Parsons and G.T. Andrews. Brillouin scattering from porous silicon-based optical bragg mirrors. Journal of Applied Physics, 111(12):123521, 2012.

[9] I.E. Psarobas, N. Papanikolaou, N. Stefanou, B. Djafari-Rouhani, B. Bonello, and V. Laude. Enhanced acousto-optic interactions in a one-dimensional phoxonic cavity. Physical Review B, 82(17):174303, 2010.

[10] E. Almpanis, N. Papanikolaou, and N. Stefanou. Breakdown of the linear acousto-optic interaction regime in phoxonic cavities. Optics express, 22(26):31595–31607, 2014.

[11] S.M. Shaban, A. Mehaney, and A.H. Aly. Determination of 1-propanol, ethanol, and methanol concentrations in water based on a one-dimensional phoxonic crystal sensor. Applied optics, 59(13):3878–3885, 2020.

[12] B. Djafari-Rouhani, S. El-Jallal, and Y. Pennec. Phoxonic crystals and cavity optomechanics. Comptes Rendus Physique, 17(5):555–564, 2016.

[13] I.M. White and X. Fan. On the performance quantification of resonant refractive index sensors. Optics Express, 16(2):1020, 2008.

[14] G.N. Aliev, B. Goller, P.A. Snow, H. Heinrich, B. Yuan, and R. Aigner. Porous silicon bulk acoustic wave resonator with integrated transducer. Nanoscale research letters, 7(1):1–6, 2012.

[15] H. Shinoda, T. Nakajima, K. Ueno, and N. Koshida. Thermally induced ultrasonic emission from porous silicon. Nature, 400(6747):853–855, 1999.

[16] P. Guiraud, S. Giordano, O. Bou-Matar, P. Pernod, and R. Lardat. Multilayer modeling of thermoacoustic sound generation for thermophone analysis and design. Journal of Sound and Vibration, 455:275–298, September 2019.

[17] M. Daschewski, R. Boehm, J. Prager, M. Kreutzbruck, and A. Harrer. Physics of thermo-acoustic sound generation. Journal of applied Physics, 114(11):114903, 2013.

[18] M. Trigo, A. Bruchhausen, A. Fainstein, B. Jusserand, and V. Thierry-Mieg. Confinement of acoustical vibrations in a semiconductor planar phonon cavity. Physical review letters, 89(22):227402, 2002.

[19] W. Theiβ, S. Henkel, and M. Arntzen. Connecting microscopic and macroscopic properties of porous media: choosing appropriate effective medium concepts. Thin Solid Films, 255(1-2):177–180, 1995.

[20] P.J. Reece, G. Lérondel, W.H. Zheng, and M. Gal. Optical microcavities with subnanometer linewidths based on porous silicon. Applied Physics Letters, 81(26):4895–4897, December 2002.

[21] M. Ghulinyan, C.J. Oton, G. Bonetti, Z. Gaburro, and L. Pavesi. Free-standing porous silicon single and multiple optical cavities. Journal of Applied Physics, 93(12):9724–9729, June 2003.

[22] C. Schinke, P. P. Christian, J. Schmidt, R. Brendel, K. Bothe, M. R. Vogt, I. Kröger, S. Winter, A. Schirmacher, S. Lim, H. T. Nguyen, and D. MacDonald. Uncertainty analysis for the coefficient of band-to-band absorption of crystalline silicon. AIP Advances, 5(6):067168, 2015.

[23] F.L. Pedrotti, L.M. Pedrotti, and L.S. Pedrotti. Introduction to optics. Cambridge University Press, 2017.

[24] J. Allard and N. Atalla. Propagation of sound in porous media: modelling sound absorbing materials 2e. John Wiley & Sons, 2009.

[25] L.M. Brekhovskikh and O.A. Godin. Acoustics of layered media i, vol. 5 of springer series on wave phenomena, 1990.

[26] W.P. Mason and T.B. Bateman. Ultrasonic-wave propagation in pure silicon and germanium. The Journal of the Acoustical Society of America, 36(4):644–652, 1964.

[27] M.B. Gitis. Sound absorption in metals at high temperatures. JETP, 40:181, 1975.

[28] S.D. Lambade, G.G. Sahasrabudhe, and S. Rajagopalan. Temperature dependence of acoustic attenuation in silicon. Physical Review B, 51(22):15861, 1995.

[29] S. Rajagopalan and D.N. Joharapurkar. Temperature dependence of the nonlinearity constant and ultrasonic attenuation in pure silicon and germanium. Journal of applied physics, 54(6):3166–3171, 1983.

[30] S. Lettieri, U. Bernini, . Massera, and P. Maddalena. Optical investigations on thermal conductivity in n-and p-type porous silicon. physica status solidi (c), 2(9):3414–3418, 2005.

[31] Z. Knittl. Optics of Thin Films (An Optical Multilayer Theory). John Wiley & Sons, 03 1976.

[32] L.G. Cencha, C. Antonio Hernández, L. Forzani, R. Urteaga, and R.R. Koropecki. Optical performance of hybrid porous silicon–porous alumina multilayers. Journal of Applied Physics, 123(18):183101, May 2018.